Published in final edited form as:
Nature. 2013 May 9; 497(7448): 205–210. doi:10.1038/nature12076.

Hierarchy of orofacial rhythms revealed through whisking and breathing

Jeffrey D. Moore[1,*], **Martin Deschênes**[2,*], **Takahiro Furuta**[3], **Daniel Huber**[4,†], **Matthew C. Smear**[4], **Maxime Demers**[2], and **David Kleinfeld**[1,5]

[1]Department of Physics, UCSD, La Jolla, CA, USA

[2]Department of Psychiatry and Neuroscience, Laval University, Quebec City, Canada

[3]Department of Morphological Brain Science, Kyoto University, Japan

[4]HHMI Janelia Farm Research Campus, Ashburn, VA, USA

[5]Section on Neurobiology, UCSD, La Jolla, CA, USA

Abstract

Whisking and sniffing are predominant aspects of exploratory behavior in rodents, yet the neural mechanisms that generate their motor patterns remain largely uncharacterized. We use anatomical, behavioral, electrophysiological, and pharmacological tools to demonstrate that these patterns are coordinated by respiratory centers in the ventral medulla. We delineate a distinct region in the ventral medulla that provides rhythmic input to the facial motoneurons that drive protraction of the vibrissae. Neuronal output from this region is reset at each inspiration by direct input from the preBötzinger complex, such that high frequency sniffing has a one-to-one coordination with whisking while basal respiration is accompanied by intervening whisks that occur between breaths. We conjecture that the respiratory nuclei, which project to other premotor regions for oral and facial control, function as a master clock for behaviors that coordinate with breathing.

Keywords

Brainstem; Bötzinger; central pattern generator; facial nucleus; preBötzinger; respiratory complex; reticular formation

Active sensing is an essential component of orofacial behavior. Animals rhythmically sniff to smell, lick to taste, and whisk to touch. The muscles involved in these patterned sensory behaviors overlap with those involved with the ingestive behaviors of chewing, swallowing,

Correspondence and requests for materials should be addressed to M.D. (martin.deschenes@crulrg.ulaval.ca) or D.K. (dk@physics.ucsd.edu). **Editorial correspondence:** David Kleinfeld, Department of Physics 0374, University of California, 9500 Gilman Drive, La Jolla, CA 92093, Office: 858-822-0342, Mobilel: 858-922-4664, Fax: 858-534-7697, dk@physics.ucsd.edu.
*Equal primary authors
Currently at Department of Neuroscience, University of Geneva, Switzerland

Author Contributions.
M.D., D.K. and J.D.M. planned the experiments and wrote the manuscript, M.D., T.F. and J.D.M. performed the rat experiments with assistance from M.D. on the histology and vibrissae tracking, D.H. performed the mouse experiments with surgical assistance from M.S., and J.D.M. analyzed the data with methodological contributions from D.K.

The authors declare no competing financial interests.

and suckling. Of critical importance, all of these behaviors share the motor plant involved in respiration and control of the upper airway. Given the essential nature of breathing and the biomechanical constraints that link the different behaviors, the coordination among orofacial behaviors constitutes a computational aspect of homeostatic control with little margin for error[1–6].

Here we investigate the issue of coordination of orofacial behaviors in the context of sniffing and whisking in rodents. These closely associated rhythmic behaviors constitute the animals' predominant activities during exploration and social interactions[7–9]. The cycle of rhythmic breathing is driven by neurons in the preBötzinger complex, which generates the inspiratory rhythm[10,11], the Bötzinger complex and parafacial respiratory groups, which shape the expiratory rhythm[5], the ventral respiratory groups, which drive the respiratory pump muscles[12], and several pools of cranial motoneurons that control the upper airway valve muscles[13]. The drive for rhythmic whisking remains to be identified. Yet whisking persists after decortication[7,14] and sensory deafferentation[7,15,16], which suggests that it too involves a rhythmic generator in the brainstem. Further, the facial motoneurons that drive the muscles involved in whisking are located immediately rostral to nuclei within the ventral medulla that generate breathing, and activity within these facial motoneurons and muscles is time-locked to breathing[17,18]. These prior results support a common neural circuitry for the rhythmic control of both breathing and whisking.

Obligatory phase-locking of whisking and breathing

Concurrent measurements of breathing and whisking in head-fixed rats reveal key aspects of their coordination (Fig. 1a,b). First, breathing over a wide range of rates can occur without substantial whisking (top and middle, Fig. 1b). To test whether whisking can also occur without breathing, we applied a puff of ammonia to the snout, which inactivates the central inspiratory drive[19] (Fig. S1) and temporarily inhibits respiration. Critically, rats can whisk during such a disruption in breathing (middle, Fig. 1b), which implies that the oscillator(s) for breathing and whisking are separately gated.

Exploratory behavior typically consists of bouts of simultaneous whisking and fast breathing, or "sniffing"[7]. Under such circumstances, fast breathing is always accompanied by a one-to-one relation with whisking (top, Fig. 1b), which is strikingly evident as the rat begins to breathe again after apnea (middle, Fig. 1b). In contrast, basal breathing is accompanied by whisks that are coincident with an inspiration, denoted "inspiratory-locked whisks", plus decrementing "intervening whisks" that occur between successive breaths (bottom, Fig 1b). This leads to an incommensurate many-to-one relation between whisking and breathing. These data imply that there are separate, or separable, oscillators for breathing and whisking, and that the breathing rhythm may reset the whisking rhythm.

The temporal relation between whisking and breathing was quantified across the complete data set (5 rats) (Fig. 1c–e). We observe that breathing occurs over a broad range of frequencies, yet has two modes (top, Fig. 1c). We define "basal respiration" as epochs with a breathing rate below 3 Hz and "sniffing" as epochs with rates above 5 Hz (top, Fig. 1c). Whisking has a broad, high frequency spectral content during both basal respiration and

sniffing (bottom, Fig. 1c). The detailed timing between whisking and breathing is revealed though a frequency-ordered plot of the correlation of whisking with breathing (Fig. 1d). Vibrissa protractions are time-locked to the onset of inspiration across the entire range of breathing frequencies; the green arrow in Figure 1d accounts for the delay between inspiratory drive to diaphragm relative to that of the upper airway[20]. Basal respiration cycles are accompanied by multiple whisks per breath, with an instantaneous whisking frequency of ~ 8 Hz for the intervening whisks (Figs. 1d & S2). Analogous results, but with an instantaneous whisking frequency of ~ 13 Hz for the intervening whisks, are observed with mice (n = 4) (Fig. S3). Lastly, phase-sensitivity analysis[21] shows that inspirations late in the whisk cycle elicit a new protraction earlier than expected (Fig. S4) and that breathing drives whisking but not *vice versa* (Fig. S5). Collectively, these data imply a unidirectional connection from the breathing oscillator[5,6,10] to a still hypothetical oscillator that generates whisking.

Facial muscles that drive whisking versus breathing rhythms

Whisking and breathing-associated nose movements share facial muscle groups[22–24]. Thus the difference in the pattern of whisking versus basal respiration (bottom, Fig. 1b) raises the issue of which muscle groups follow the sequence of motor commands associated with whisking[25] as opposed to those associated with breathing[1]. In particular, protraction of the vibrissae is primarily driven by intrinsic papillary muscles that wrap around the individual vibrissa follicles (Fig. 2a), while retraction involves viscoelastic forces as well as translation of the mystacial pad[15] that is driven by the “extrinsic” *nasolabialis* and *maxillolabialis* muscles[25] (Fig. 2a). This determination of motor control is essential to understand the premotor brainstem circuits that drive different aspects of whisking.

We observe that the activity of the intrinsic muscles, measured via their differential electromyogram (∇EMG), leads protraction for both sniffing (Fig. 2b) and basal respiration (Fig. 2c). The *nasolabialis* muscle, also measured via its ∇EMG, is active for every whisk during sniffing (Fig. 2b) yet is only active for inspiratory-locked whisks during basal breathing (Fig. 2c). The timing and extent of this process was quantified in terms of the population averaged cross-correlations between the different features of whisking and the |∇EMG| of the different muscle groups (3600 inspiratorylocked and 500 intervening whisks in two rats). This analysis indicates consistent modulation of the intrinsic |∇EMG| during both inspiratory and intervening whisks but modulation of the extrinsic |∇EMG| activity only for inspiratory whisks (Fig. S6), thus extending past results on the role of extrinsic muscles[15,25]. These data imply that protraction is driven by the hypothesized whisking oscillator, while retraction of the mystacial pad is controlled, at least in part, by respiratory patterning circuitry.

The intermediate reticular formation contains a region that signals protraction of the vibrissae

The coordination of whisking with breathing and the resetting of whisking by inspiration suggests that a vibrissa pattern generator is driven by respiratory nuclei, which are known to lie in the ventral medulla[1]. Further, the difference in the basal respiration and whisking

patterns provides a signature to discriminate between breathing and potential whisking neuronal centers (bottom, Fig. 1b). We recorded multiunit spiking activity in the area of the preBötzinger, Bötzinger and adjoining ventral and parafacial respiratory regions (Fig. 3a–c) identified each recording site by subsequent reconstruction (Fig. 3d,e). The functional attributes of each multi-unit signal were assigned as inspiratory/protraction (32 units), expiratory/retraction (29 units), or whisking (5 units) based on their patterns of activity during whisking and sniffing (Fig. 3f). We find that units that have a similar phase preference also lie in close spatial proximity (Fig. 3d–f). Specifically, multiunit activity in the region of the preBötzinger complex and the ventral respiratory group occurred in phase with inspiration and protraction of inspiratory-locked whisks (Fig. 3a, red dots in Fig. 3d,e). Multiunit activity in the region of the Bötzinger complex and the parafacial respiratory group occurred in approximate phase with expiration and retraction of inspiratory-locked whisks (Fig. 3b, yellow dots in Fig. 3d,e). In neither case did the activity track the intervening whisks. In contrast, we located a subset of units in the intermediate band of the reticular formation (IRt) whose spiking was tightly phase-locked to the protraction of both inspiratory-locked and intervening whisks (Figs. 3c & S7). These units are potential pre-motor drivers of the intrinsic muscles that serve rhythmic whisking (Fig. 2a) and are henceforth referred to as "whisking units". They are located in the ventral part of the IRt, medial to the *ambiguus* nucleus *pars semicompacta* and near the preBötzinger complex (blue dots in Fig. 3d,e). We denote this new region the vibrissa zone of the IRt (vIRt).

The phase of the neuronal activity of the above three classes of rhythmically spiking units with respect to behavior was compared with that of the intrinsic (green bars in Fig. 3f) and *nasolabialis* $|\nabla EMG|$ (black bars in Fig. 3f). First, there is a slight phase lead between the majority of whisking units and the intrinsic muscles. Second, the activity of inspiratory/protraction units tends to lead that of the whisking units, which is particularly robust during near synchronous whisking and sniffing (Fig. 3f). These data are consistent with inspiratory/protraction units in or near the preBötzinger complex resetting a group of rhythmic whisking units in the vIRt to initiate protraction. In addition, expiratory/retraction units exhibit a phase shift between sniffing and basal respiration that is paralleled by a concurrent shift in activation of the *nasolabialis* muscle (Fig. 3f).

Activation of cells in the vibrissa zone of the IRt leads to autonomous whisking

The hypothesis that whisking in the vIRt constitute the oscillator for whisking predicts that activation of this region will lead to prolonged autonomous activity. Indeed, microinjection of the glutamate receptor agonist kainic acid in the vicinity of the vIRt is a salutary means to induce prolonged rhythmic muscular activation (Figs. 4a & S8) and coordinated vibrissa protraction (Fig. S9), near 10 Hz, in the lightly anesthetized headfixed rat (Fig. 4b & Movie S1). The frequency of whisking decreases over time, and the amplitude increases, as the effect of anesthesia declines, while the frequency of breathing remains constant (Fig. 4c). This implies that the chemical activation is sufficiently strong to decouple rhythmic protraction from breathing (Fig. S10). Quantitatively, the modulation depth of protraction with breathing was less than 0.01 and insignificant for all but one case (11 epochs across

three rats), compared with 0.08 for basal respiration and 0.26 for sniffing in awake animals. Lastly, consistent with the conclusions from the EMG studies (Fig. 2d), the mystacial pad moves in synchrony with breathing (Fig. 4b).

Chemical activation of rhythmic whisking, with a frequency incommensurate with that of breathing, provides an opportunity to stably record from units whose firing times were coherent with rhythmic protraction (inserts, Fig. 4d). We identified units that spiked in synchrony with protraction, as in the case of units identified during intervening whisks in the behaving animal (Fig. 3c–f), as well as units that spiked in anti-phase (32 units across four rats) (Fig. 4d). Microinjection of Neurobiotin™ at the recording site (Fig. 4e1) resulted in anterograde labeling of axon terminals in the ventrolateral part of the facial nucleus, where motoneurons that innervate the intrinsic muscles are clustered (Fig. 4e2). The recording sites were located medial to the *ambiguus* nucleus (Fig. 4f), similar to the region localized by recording in behaving animals (Fig. 3d,e).

Lesion of the vibrissa zone of the IRt extinguishes ipsilateral whisking

The above results provide evidence for the sufficiency of neurons in the vIRt to drive rhythmic protraction. We now consider the necessity of the vIRt for rhythmic motion and test if a lesion to this zone suppresses whisking. First, small electrolytic lesions of the IRt medial to the *ambiguus* nucleus abolish whisking on the side of the lesion, while whisking persists on the contralateral side (Fig. 5a & Movie S2). Neither basal respiration nor sniffing is affected by the lesion. Further, the suppression of whisking appeared permanent as no recovery was observed up to 10 days after the lesion. Qualitatively similar results were found with ibotenic acid or Sindbis viral lesions (Fig. S11), which indicates that the abolition of whisking is not attributable to severed axons of passage.

The spatial specificity of the ablations was assessed by lesioning various regions in the pons and medulla in an ensemble of animals (head-fixed: three electrolytic; free-ranging: 16 electrolytic, one ibotenic acid, and five Sindbis). Lesions made in the dorsal part of IRt, in the parvocellular reticular formation, in the paragigantocellular reticular formation, or in the caudal part of the medullary reticular formation excluding the preBötzinger complex, only minimally affected whisking (Fig. 5d). Critically, lesions within the vIRt that were as small as 200 μm in diameter were sufficient to severely impair whisking on the ipsilateral side (Figs. 5a,e). We conclude that units in the vIRt play an obligatory role in the generation of whisking.

Anatomical connections that define the circuit for rhythmic whisking

The behavioral (Figs. 1,2) and physiological data (Figs. 3–5) suggest that cells in inspiratory nuclei reset an oscillatory network of whisking units in the vIRt that can drive protraction of the vibrissa concurrent with each inspiration. We used tract tracing methods to assess this hypothesized connection. Injections of biotinylated dextran amine (BDA) into the preBötzinger complex, identified by the phase relation of units relative to breathing (two rats) (Fig. 6a$_1$), led to dense anterograde labeling in the IRt medial to the *ambiguus* nucleus (Fig. 6a$_2$), including a number of axon terminals (Fig. 6a$_3$). This corresponds to the same region in which we observed whisking units (Figs. 3d,e & 4e–h) and where lesions

extinguished ipsilateral whisking (Fig. 5e). These results support a direct connection from the preBötzinger complex to the vIRt.

We next delineated the projections from neurons in the vIRt to facial motoneurons (Fig. $4g_2$). Neurobiotin™ (three rats) or Fluoro-Gold™ (two rats) was injected in the lateral aspect of the facial nucleus (Figs. $6b_1$ & S12). We observed a cluster of retrogradely labeled cells in the IRt that lie medial to the *ambiguus* nucleus (Fig. $6b_2$). A detailed map of the location of cells that were retrogradely labeled from an injection in the lateral aspect of the facial nucleus (1300 cells in one rat) reveals a rostrocaudal band of cells in the IRt; we identify this region as vIRt (Figs. 6c & S12). *In toto*, these and previous[26,27] patterns of neuronal labeling in the IRt support a direct connection from the vIRt to the facial nucleus and substantiate the role of the vIRt as a premotor nucleus.

The neurotransmitter content of neurons in the vIRt that project to the facial motoneurons was assessed by the combination of retrograde labeling and *in situ* hybridization[28] (Figs. S13 & S14). We find a fractional contribution of 0.12 ± 0.02 (mean ± SE; 259 cells in 3 rats) glutamatergic, 0.85 ± 0.02 (303 cells) glycinergic, and 0.53 ± 0.03 (237 cells) Gaba-ergic neurons. These data support either monosynaptic excitatory transmission via glutamate receptors and via glycine NR1/NR3b receptors[29] or monosynaptic inhibitory transmission via glycine and Gaba receptors in the presence of a tonic excitatory drive.

The involvement of the *nasolabialis* muscle during inspiratory-locked whisks, but not intervening whisks, suggests that retraction of the mystacial pad is controlled by units in the Bötzinger/parafacial complex (Figs. 2c, 3b & 4b). These units are phaselocked with expiration (Figs. 3f & 4f). The Bötzinger/parafacial region is in close proximity to the facial nucleus[1] and is reported to modulate the activity of facial motoneurons[18,30] that drive the *nasolabialis* muscle[31]. In support of a direct connection from the Bötzinger complex to facial motoneurons, we observed that the map of retrogradely labeled projections to the facial nucleus shows strong labeling (Fig. 6c). In addition, small injections of Neurobiotin™ that were made in the parafacial region (three rats) (Fig. 6d1) labeled of axon terminals specifically in the dorsolateral part of the facial nucleus, where motoneurons that innervate the extrinsic muscles are clustered (Fig. 6d2). This result supports the conclusion that retraction of the vibrissae is at least partially mediated by neurons in Bötzinger/parafacial region.

Discussion

We have identified units in a newly defined zone of the intermediate band of the reticular formation in the medulla, denoted vIRt, that oscillate in phase with motion of the vibrissae (Fig. 7a). This zone functions as the premotor pattern generator for rhythmic whisking and is part of a larger circuit whereby cells in nuclei that are obligatory for inspiration[11,32,33] reset the phase of vIRt units with each breath (Fig. 7b). Thus, whisking during sniffing is effectively driven on a cycle-by-cycle basis by the inspiratory rhythm generator, while intervening whisks between successive inspirations result from oscillations of the whisking units in vIRt. Retraction of the vibrissae by extrinsic muscles in the mystacial pad is likely

controlled by nuclei that lie immediately caudal to the facial nucleus and are active during expiration.

Our results bear on the generation of other rhythmic orofacial behaviors, for which licking is particularly well described. First, tongue protrusions are coordinated with the respiratory cycle[34]. Second, the hypoglossal premotoneurons are concentrated in the IRt dorsomedially to the preBötzinger complex[3,35], and are driven by bursts of spikes that are locked to inspiration[36]. Third, the output of units in the hypoglossal IRt zone locks to rhythmic licking[37]. Lastly, infusion of an inhibitory agonist into the IRt blocks licking[38]. These past results are consistent with a model in which preBötzinger units reset the phase of bursting in a network of hypoglossal premotor neurons in the IRt zone, in parallel with our circuit for whisking (Fig. 7b). Serotonergic and other modulatory inputs may serve to gate and accelerate all of these rhythms[39–43].

The common architecture of the control circuits for whisking (Fig. 7b) and licking[3] supports the primary role of breathing in the coordination of orofacial behaviors. In the absence of interruptions, such as from swallowing[44] or aversive stimuli[19], we propose that the inspiratory pattern generator broadcasts a master clock signal to the various patterning circuits throughout the IRt and nearby zones (Fig. 7c). Coordination by this breathing clock can ensure that these rhythmic behaviors, which share muscle groups, do not confound each other. It is a further possibility that the breathing clock serves to perceptually bind olfactory and tactile sensory inputs.

ONLINE METHODS

Animals

Thirty-seven female Long Evans rats (250 to 350 g, Charles River) were used for behavioral and electrophysiological experiments, an additional 25 rats of mixed sex were used solely for lesion studies, and 13 female rats were used for purely anatomical studies. Four adult mice, two male C57BL/6J and two female ChR2-MBD[46] were used for behavioral studies. Experimental protocols were carried out in accordance with federally prescribed animal care and use guidelines and were approved by the Institutional Animal Care and Use Committees at the University of California in San Diego, Laval University, and Janelia Farms Research Center.

Preparation

Head-fixed rats—Rats were habituated to body restraint for 5 days, then implanted with a custom-built head restraining mount[45] and a thermocouple (K-type; Omega Engineering, CT) in the nasal cavity[47]. Surgical procedures were carried out in animals anesthetized with ketamine (90 mg/kg) / xylazine (5 mg/kg). In brief, a craniotomy was performed over the cerebellum, and a plastic chamber was centered over the opening and secured with acrylic cement. The craniotomy was filled with silicone gel (no. 3–4689; Dow Corning, MI). In two animals, Teflon-coated tungsten wires were inserted in the vibrissa pad to record activity of the intrinsic muscles and of the nasolabialis muscle[15,25]. Rats were allowed to recover for two days before the onset of behavioral experiments. During the recording sessions, rats

were placed inside a body-restraining cloth sack and rigid tube, and the animals were head-restrained[45]. All vibrissae except numbers C2 or D2 were cut at the base and movement of the intact vibrissa was recorded with videography. Rats were coaxed to whisk by presenting food or bedding from the home cage[48]. Lastly, in some experiments, a tube was placed in front of the snout to deliver one or two two-second puffs of air saturated with ammonia while the animal whisked.

Head-fixed mice—Mice were implanted with a titanium bar for head fixation[49] and with a stainless steel cannula to measure breathing as previously described[50]. The mice were allowed to recover for 10 days prior to behavioral experiments.

Recording and analysis

Whisking—Vibrissa motion in head-fixed rats was monitored one of several ways with a Basler A602f camera at a spatial resolution of 120 μm/pixel or an NMOS linear sensor (S3904-2048Q; Hamamatsu, PA). For behavioral measurements, 360x250 pixel planar images were acquired at 250 Hz with a white light emitting diode backlight for trials of 10 s each. Vibrissa angle was tracked by fitting a line to the spatially contiguous pixels comprising the initial 5 mm segment of the vibrissa base. For measurements in conjunction with extracellular recording from brainstem, we used either the Basler A602f camera in line-scan mode with a 1 kHz scan rate or the NMOS linear sensor and imaged motion along a line that was 5 to 10 mm from the edge of the mystacial pad. Pixel intensity along the line was thresholded and the centroid of the detected vibrissa was converted to a voltage proportional to pixel position in real time.

Vibrissa motion in freely moving rats with one or more vibrissae in the C or D-row was monitored with a HiSpec 2G Mono camera (Fastec Imaging, CA) at a 250 Hz frame rate, or a Powershot SX260HS camera at a 120 Hz frame rate (Canon, NY). Rats were placed in a raised, clear plastic box with a passageway that allowed them to perch in search of their home cage, located 20 cm away. Trained animals craned across the gap and sniffed and whisked vigorously[48]. Vibrissa motion was tracked with commercial software (ProAnalyst, Xcitex Inc., MA), and previously described algorithms[51].

Vibrissa motion in head-fixed mice with vibrissae in the C-row was recorded with a high-speed CMOS camera (EOSENS CL; Mikrotron) through a telecentric lens (0.36×; Edmund Optics; NJ). Streampix 3 software (Norpix, Quebec) was used to acquire the images, 640×352 pixels at a spatial resolution of 24 μm per pixel. The vibrissae were illuminated from below with collimated infrared light from a high-power light emitting diode (640nm; Roithner, Vienna). Vibrissa motion was tracked with automated procedures[49].

The extracted vibrissa movements for all cases were separated into single whisks by band-pass filtering the position traces between 3 and 25 Hz with a 3-pole Butterworth filter run in forwards and backwards directions and applying the Hilbert transform[52]. Individual candidate whisks were identified by phase resets of the Hilbert transform, and were accepted only if the minimum-to-maximum amplitude exceeded 5°and the whisk lasted less than 250 ms. The onset time of each whisk was defined as the time at which the vibrissa angle exceeded 10 % of the minimum-to-maximum amplitude.

Electromyography—Muscular activity was monitored in different muscle groups, and the integrated envelope of the EMG activity, denoted |∇EMG|, was computed as previously described[15,25]. We then computed the cross-correlation between protraction onset times and the |∇EMG|. The 95 % confidence intervals were obtained by re-sampling with replacement 1000 times from the set of protraction onset times and computing the cross-correlation with the re-sampled dataset.

Breathing—Respiration-related changes in temperature or pressure sensors were digitized and band pass filtered between 1 and 15 Hz with a 3-pole Butterworth filter run backwards and forwards in time. Onset times for inspiratory events were defined as described above for whisking.

In rats, respiration-related changes in temperature were verified to be synchronous with chest expansion, which are presumed to track diaphragm movements, as measured with a piezoelectric strap around the abdomen in separate experiments.

Neuronal signaling in awake, behaving rats—Multiunit neuronal activity was recorded in the ventral medulla with quartz micropipettes, 10 to 25 μm tip diameter, filled with 2 % (w/v) Chicago sky blue (Sigma, MO) in artificial cerebral spinal saline, or with tungsten microelectrodes (1 MΩ impedance; Microprobes, MD). Electrode position was controlled by a motorized manipulator (model MP-285, Sutter, CA). Units were held for one to twenty minutes. Signals were amplified, band-pass filtered between 300 Hz and 6 kHz and sampled at 20 or 40 kHz. The noise level, σ, was defined as the standard deviation of the voltages recorded over the entire time the electrode was maintained at a recording site. Multiunit spike events were defined as voltage fluctuations that exceeded 3.5-times σ.

One or more recording sites in each session were marked with an extracellular deposit of Chicago sky blue by electrophoresis; − 10 to − 50 μA with 10 s pulses spaced every 20 s for five minutes, or by electrolytic lesion with 40 to 80 μA applied for three intervals of 2 to 5 s. Rats were deeply anesthetized at the end of the session and perfused with phosphate buffered saline (PBS), followed by perfusion with 4 % (w/v) paraformaldehyde in PBS. Brains were post-fixed overnight in 4 % paraformaldehyde in PBS, cryoprotected in 30 % (w/v) sucrose in PBS, and sectioned along the sagittal or coronal plane at a thickness of 60 μm with a freezing microtome. Sections were stained with either Neutral red, Neurotrace™ blue (fluorescent Nissl; Invitrogen, CA), or cytochrome oxidase[53].

Kainic acid-induced whisking—Microinjections of kainic acid were made through quartz or glass micropipettes, 10 to 15 μm in diameter, in rats anesthetized with ketamine/xylazine as described above. Injections were targeted to the approximate vibrissa region of the intermediate band of the reticular formation (vIRt) as defined in our anatomical studies (Fig. 6) using stereotaxic coordinates. Kainic acid was prepared as 1 % (w/v) in Tris buffer, pH 8.2 and delivered by iontophoresis with −500 nA, 250 ms pulses spaced every 500 ms for 600 s. In several experiments, biotinylated dextran amine (MW 3000; Invitrogen) prepared as 2 % (w/v), was added to the solution to facilitate labeling of the injection site.

Rats were secured with a head-fixed mount and their vibrissae were monitored with a camera in linescan mode (Basler A602f). Coordinated, rhythmic vibrissa movements typically began 15 to 30 minutes after the kainic acid injection, at which point all vibrissae except number C2 or D2 were trimmed. Individual whisks were detected, as described above, with the exception that the threshold for detecting a whisk was set to 1°.

Single and multiunit recordings in the vicinity of the site of the kainic acid injections were made in a subset of rats using glass microelectrodes with 2 to 3 μm tips back-filled with Neurobiotin™ (Vector Labs, CA), prepared as a 2 % (w/v) solution in 500 mM potassium acetate. These pipettes served for both recording and labeling of the recording site. The centroid of injection sites that induced whisking varied by up to 1 mm relative to the actual anatomical location of the vIRt, consistent with variability in stereotaxic coordinates between rats[54] and the rapid diffusion of kainic acid. We thus made multiple penetrations offset by at most 100 μm of each other to locate units whose spiking was locked to whisking following the kainic acid injection. The depth of each unit along a penetration was noted, and at the end of a subset of the experiments the recording site was labeled via iontophoresis; + 50 to 100 nA, 2 s pulses spaced every 4 s for 1000 s. The animals were perfused two hours after the injection.

Coherence and correlation analysis—To assess the degree and statistical significance of correlation between whisking and breathing events (Fig. 1d), we computed the cross correlation between whisk onset times and breath onset times separately for basal respiration, with rates < 3 Hz, and sniffing, with rates > 5 Hz. The maximum lag for the cross-correlation computed in each case was bounded by the minimum breathing period. Statistical significance was assessed by performing a one sample Kolmogorov-Smirnov test versus the uniform distribution expected by chance. Correspondingly, we define the modulation depth of the cross correlation as the corresponding Kolmogorov-Smirnov test statistic.

Additional analyses were performed in the frequency domain to assess the spectral content and synchrony between whisking, breathing, and spiking activity. For experiments in awake animals, whose behavior exhibited interleaved bouts of basal respiration, sniffing and whisking, our data was segmented as follows. First, “inspiratory” whisks were defined as those whisks whose onset occurred within 100 ms of an inspiration, while intervening whisks were defined as whisks that did not occur within 100 ms of the closest onset of inspiration. Next, behavioral epochs were classified as “basal respiration” when the instantaneous respiratory frequency was less than 3 Hz, “sniffing” for periods when the instantaneous respiratory frequency was greater than 5 Hz, “inspiratory whisking” for periods of successive inspiratory whisks, and “intervening whisking” for periods of successive intervening whisks during “basal respiration”. Bouts of these behaviors were divided into non-overlapping segments of a predetermined length, *i.e*., 1 s for basal respiration, 500 ms for sniffing and inspiratory whisking, and 300ms for intervening whisking. For each segment we extracted the relevant behavioral signal, *i.e*., inspiration onset times for basal respiration and sniffing and vibrissa position for inspiratory and intervening whisking, and the relevant physiological signal, *i.e*., the $|\nabla EMG|$ or the multiunit spike times.

The Chronux toolbox (www.chronux.org) was used to compute the spectral coherence between these respective behavioral and physiological signals, averaged over all segments with a time-bandwidth product of one. We report the magnitude and phase of the coherence at the peak frequency of the behavior (Fig. 1c), *i.e*., 2 Hz for basal respiration, 6 Hz for sniffing and inspiratory whisking, and 8 Hz for intervening whisking. The whisking and breathing analyses are normalized so that a phase of zero corresponds to the onsets of protraction and inspiration, respectively, as defined above.

For experiments in anesthetized animals with pharmacologically induced whisking, we computed the spectral coherence between vibrissa position and either spike times or |∇EMG| irrespective of breathing, averaged over all 2 s segments with a time-bandwidth product of 2. We report the magnitude and phase of the coherence at the peak frequency whisking, which varied between experiments. The analysis is normalized as above, where phase zero corresponds to the onset of protraction.

Medullary lesions and whisking

Electrolytic lesions were made with metal microelectrodes (0.5 MΩ; FHC Inc., ME) by passing direct current of + 40 to 80 μA for 5 s at multiple nearby spatial locations. In select cases the lesions were performed with glass pipettes in head-fixed animals immediately after unit recordings in the vIRt. Ibotenic acid lesions were made by pressure injection of approximately 300 nL of ibotenic acid, prepared as 1 % (w/v) in physiological saline. Sindbis virus lesions were made by pressure injection of approximately 100 to 300 nL of viral vector[55] (~3×10^3 infectious particles/μL) using glass micropipetts with 30 μm diameter tips. After the animal was allowed to recovery from surgery, high speed videography of vibrissa motion on both sides of the face in both head-fixed and freely-moving animals was performed. Vibrissae were tracked and individual whisks were identified based on the motion on the contralateral side, as described above. The mean amplitude of the Hilbert transform over the period of each whisk was calculated for both the ipsilateral and contralateral sides.

Anatomy

Anterograde and retrograde labeling—All tracer injections were made under ketamine/xylazine anesthesia, as above, with concurrent monitoring of respiration. Cells in the Bötzinger/parafacial complex were labeled with Neurobiotin™ (Vector Labs, CA), prepared as a 2 % (w/v) solution in 500 mM potassium acetate. Glass microelectrodes with 4 to 5 μm tips served for both recording and injection. Bötzinger cells were identified by their expiratory-related activity and Neurobiotin™ was delivered by iontophoresis; + 50 to 100 nA, 2 s pulses spaced every 4 s for 1000 s. The animals were perfused after 90 minutes of recovery.

Cells in the preBötzinger complex were similarly identified by their inspiratory-related activity and labeled with biotinylated dextran amine (10 kD MW; Invitrogen), prepared as a 2 % (w/v) solution in 500 mM potassium acetate. Biotinylated dextran amine was delivered by iontophoresis using glass microelectrodes with 8 to 10 μm tips; + 200 nA, 2 s pulses spaced every 4 s for 1000 s. The animals were perfused after 2 days of recovery.

Cells that projected to the facial motor nucleus were labeled retrogradely with Neurobiotin™, prepared as a 2 % (w/v) solution in 10 mM sodium citrate buffer at pH 3.0 using glass microelectrodes with 20 μm diameter tips. The location was confirmed by microstimulation, +5 to 10 μA pulses, 100 μs in width, delivered at 100 Hz, that led to ~ 2° movements of one or more vibrissae. Neurobiotin™ was delivered by iontophoresis; + 300 nA, 2 s pulses spaced every 4 s for 1000 s. The animals were perfused after three hours of recovery. Complementary studies involved the use of Fluoro-Gold™ (Fluorochrome, Denver), prepared as a 1 % (w/v) in 0.1 M cacodylate buffer at pH 7.0, delivered as above but with the animals perfused after two days.

After perfusion, brains were post-fixed for two hours and cryoprotected in 30 % (w/v) sucrose for 12 hours. Then the brainstems were isolated and cut in the coronal or sagittal plane at a thickness of 50 μm on a freezing microtome. Neurobiotin™ and BDA were revealed with ABC Elite and SG kits (Vector Labs) or with streptavidin-Alexa 488 (1:200 dilution; Invitrogen). Fluoro-Gold™ was revealed by immunohistochemistry (1:5000 dilution; Millipore, CA). Sections were then counterstained with either Neutral red, immunostained for choline acetyltransferase (1:1000 dilution of α-ChAt; Millipore), or reacted for cytochrome oxidase.

Lesion anatomy—Animals lesioned with the Sindbis viral vector, in which we observed a severe deficit in whisking, were perfused immediately after video recordings; this corresponded to 50 to 75 hours after injection of the virus. Animals that did not exhibit a deficit were perfused after 4 to 6 days. Animals lesioned electrolytically or with ibotenic acid were perfused 2 to 10 days after the procedure. For electrolytic lesions, 60 μm coronal or sagittal sections were stained for neutral red. For ibotenic acid and Sindbis viral lesions, 30 μm coronal or sagittal sections were immunostained for neuronal nuclear protein (1:200 dilution of α-NeuN; Millipore). For Sindbis viral lesions, alternate sections were stained for myelin (Luxol fast blue; Sigma) and cell bodies (neutral red).

Mapping—Histological sections were scanned at 1 μm spatial resolution using a Nanozoomer (Hamamatsu) digital slide scanner. The stereotaxic recording sites were superimposed on the scans according to their distance to the nearest labeled site. Sections containing Chicago sky blue deposits and associated recording sites were aligned by manual rotation and translation with an atlas of sagittal Nissl sections (brainmaps.org). The outlines of prominent medullary structures including the facial nucleus, lateral reticular nucleus, *ambiguus* nucleus and inferior olive were traced with Neurolucida™ (Microbrightfield, VT) software, and sections were aligned based on these anatomical borders to yield a three-dimensional reconstruction of the medulla. The extents of brainstem lesions were similarly mapped onto standard frontal sections[56].

Combined anatomy and in situ hybridization

Retrograde labeling and in-situ hybridization—Tracer injections were made under ketamine/xylazine anesthesia. Fluoro-Gold™, 4 % (w/v) in saline, was injected into the lateral part of the facial nucleus by passing 500 nA current pulses, 7 s in duration, every 14 s for 300 s using glass microelectrodes with 20 μm diamters tips. After a survival periods of

48 hours, rats were perfused as described above. After fixation, brains were removed, the brainstem isolated, cryoprotected with diethylpyrocarbonate-treated sucrose, and cut into 30-μm-thick sagittal sections on a freezing microtome for *in situ* hybridization[57].

Cell counting—Retrogradely labeled cells in sections processed for *in situ* hybridization were counted under confocal microscopy with a 40× objective, as described[28]. Approximately ten fields were scanned in a grid-like manner across the vIRt, as defined in our other anatomical tracing experiments (Fig. S8). For each field, a stack of 5 to 10 optical sections were acquired, and counts were made from the stacked images.

Supplementary Material

Refer to Web version on PubMed Central for supplementary material.

Acknowledgments

We thank A. Kepecs and F. Wang for sharing unpublished work, and these colleagues along with M. S. Fee, J. L. Feldman, H. J. Karten, P. M. Knutsen, D. M. Matthews and K. Svoboda for discussions. We further thank K. Svoboda for sponsorship of the mouse experiments, M. Agrochao and B. el Jundi for assistance with these experiments, T. Ito and D. L. Oliver for use of their GlyT2 probe, K. K. Baldwin for the gift of the Sindbis viral vector, and K. Yang for assistance with behavioral training. We are grateful to the Canadian Institutes of Health Research (grant MT-5877), the Howard Hughes Medical Institute, the Japan Society for the Promotion of Science (KAKENHI grants 23135519 and 24500409), the National Institutes of Health (grants NS058668, NS066664 and NS047101), and the US-Israeli Binational Science Foundation (grant 2003222).

References

1. Smith JC, Abdala APL, Rybak IA, Paton JFR. Structural and functional architecture of respiratory networks in the mammalian brainstem. Philosophical Transactions of the Royal Society of London B. 2009; 364:2577–2587.
2. Nakamura Y, Katakura N. Generation of masticatory rhythm in the brainstem. Neuroscience Research. 1995; 23:1–19. [PubMed: 7501294]
3. Travers JB, Dinardo LA, Karimnamazi H. Motor and premotor mechanisms of licking. Neuroscience and Biobehavioral Reviews. 1997; 21:631–647. [PubMed: 9353796]
4. Alheid GF, McCrimmon DR. The chemical neuroanatomy of breathing. Respiratory Physiology & Neurobiology. 2008; 164:3–11. [PubMed: 18706532]
5. Feldman JL, Del Negro CA, Gray PA. Understanding the rhythm of breathing: So near, yet so far. Annual Review of Physiology. 2013; 75:423–452.
6. Garcia AJ, Zanella S, Koch H, Doi A, Ramirez JM. Networks within networks: The neuronal control of breathing. Progress in Brain Research. 2011; 188:31–50. [PubMed: 21333801]
7. Welker WI. Analysis of sniffing of the albino rat. Behaviour. 1964; 12:223–244.
8. Brecht M, Freiwald WA. The many facets of facial interactions in mammals. Current Opinion in Neurobiology. 2011 Epub ahead of print.
9. Vincent SB. The function of the vibrissae in the behavior of the white rat. Behavior Monographs. 1912; 1:7–81.
10. Smith JC, Ellenberger HH, Ballanyi K, Richter DW, Feldman JL. Pre-Botzinger complex: A brainstem region that may generate respiratory rhythm in mammals. Science. 1991; 254:726–729. [PubMed: 1683005]
11. Tan W, Janczewski WA, Yang P, Shao XM, Callaway EM, Feldman JL. Silencing preBötzinger Complex somatostatin-expressing neurons induces persistent apnea in awake rat. Nature Neuroscience. 2008; 11:538–540.
12. Dobbins EG, Feldman JL. Brainstem network controlling descending drive to phrenic motoneurons in rat. Journal of Comparative Neurology. 1994; 347:64–86. [PubMed: 7798382]

13. Bieger D, Hopkins DA. Viscerotopic representation of the upper alimentary tract in the medulla oblongata in the rat: the nucleus ambiguus. Journal of Comparative Neurology. 1987; 262:546–562. [PubMed: 3667964]

14. Semba K, Komisaruk BR. Neural substrates of two different rhythmical vibrissal movements in the rat. Neuroscience. 1984; 12:761–774. [PubMed: 6472619]

15. Berg RW, Kleinfeld D. Rhythmic whisking by rat: Retraction as well as protraction of the vibrissae is under active muscular control. Journal of Neurophysiology. 2003; 89:104–117. [PubMed: 12522163]

16. Gao P, Bermejo R, Zeigler HP. Vibrissa deaffentation and rodent whisking patterns: Behavioral evidence for a central pattern generator. Journal of Neuroscience. 2001; 21:5374–5380. [PubMed: 11438614]

17. Huangfu D, Koshiya N, Guyenet PG. Central respiratory modulation of facial motoneurons in rats. Neuroscience Letters. 1993; 151:224–228. [PubMed: 8506084]

18. Onimaru H, Kumagawa Y, Homma I. Respiration-related rhythmic activity in the rostral medulla of newborn rats. Journal of Neurophysiology. 2006; 96:55–61. [PubMed: 16495360]

19. Lawson EE, Richter DW, Czyzyk-Krzeska MF, Bischoff A, Rudesill RC. Respiratory neuronal activity during apnea and other breathing patterns induced by laryngeal stimulation. Journal of Applied Ohysiology. 1991; 70:2742–2749.

20. Fukuda Y, Honda Y. Differences in respiratory neural activities between vagal (superior laryngeal), hypoglossal, and phrenic nerves in the anesthetized rat. Japanese Journal of Physiology. 1982; 32:387–398. [PubMed: 6813545]

21. Ermentrout GB, Kleinfeld D. Traveling electrical waves in cortex: Insights from phase dynamics and speculation on a computational role. Neuron. 2001; 29:1–12. [PubMed: 11182073]

22. Sherrey JH, Megirian D. State dependence of upper airway respiratory motoneurons: Functions of the cricothyroid and nasolabial muscles of the unanesthetized rat. Electroencephalography and Clinical Neurophysiology. 1977; 43:218–228. [PubMed: 69532]

23. Haidarliu S, Golomb D, Kleinfeld D, Ahissar E. Dorsorostral snout muscles in the rat subserve coordinated movement for whisking and sniffing. Anatomical Record. 2012 in press.

24. Dorfl J. The musculature of the mystacial vibrissae of the white mouse. Journal of Anatomy. 1982; 135:147–154. [PubMed: 7130049]

25. Hill DN, Bermejo R, Zeigler HP, Kleinfeld D. Biomechanics of the vibrissa motor plant in rat: Rhythmic whisking consists of triphasic neuromuscular activity. Journal of Neuroscience. 2008; 28:3438–3455. [PubMed: 18367610]

26. Takatoh J, Nelson A, Zhou X, Bolton MM, Ehlers MD, Arenkiel BR, Mooney R, Wang F. New modules are added to vibrissal premotor circuitry with the emergence of exploratory whisking. Neuron. 2013; 77:346–360. [PubMed: 23352170]

27. Isokawa-Akesson M, Komisaruk BR. Difference in projections to the lateral and medial facial nucleus: Anatomically separate pathways for rhythmical vibrissa movement in rats. Experimental Brain Research. 1987; 65:385–398. [PubMed: 3556466]

28. Furuta T, Timofeeva E, Nakamura K, Okamoto-Furuta K, Togo M, Kaneko T, Deschênes M. Inhibitory gating of vibrissal inputs in the brainstem. Journal of Neuroscience. 2008; 28:1789–1797. [PubMed: 18287495]

29. Chatterton JE, Awobuluyi M, S PL, Takahashi H, Talantova M, Shin Y, Cui J, Tu S, Sevarinok KA, Nakanishi N, Tong G, Lipton SA, Zhang D. Excitatory glycine receptors containing the NR3 family of NMDA receptor subunits. Nature. 2002; 415:793–798. [PubMed: 11823786]

30. Pagliardini S, Janczewski WA, Tan W, Dickson CT, Deisseroth K, Feldman JL. Active expiration induced by excitation of ventral medulla in adult anesthetized rats. Journal of Neuroscience. 2011; 31:2895–2905. [PubMed: 21414911]

31. Klein B, Rhoades R. The representation of whisker follicle intrinsic musculature in the facial motor nucleus of the rat. Journal of Comparative Neurology. 1985; 232:55–69. [PubMed: 3973083]

32. Gray PA, Hayes JA, Ling GY, Llona I, Tupal S, Picardo MC, Ross SE, Hirata T, Corbin JG, Eugenín J, Del Negro CA. Developmental origin of preBötzinger complex respiratory neurons. Journal of Neuroscience. 2010; 30:14883–148895. [PubMed: 21048147]

33. Bouvier J, Thoby-Brisson MNR, Dubreuil V, Ericson J, Champagnat J, Pierani AAC, Fortin G. Hindbrain interneurons and axon guidance signaling critical for breathing. Nature Neuroscience. 2010; 13:1066–1074.
34. Welzl H, Bures J. Lick-synchronized breathing in rats. Physiological Behavior. 1977; 18:751–753.
35. Koizumi H, Wilson CG, Wong S, Yamanishi T, Koshiya N, Smith JC. Functional imaging, spatial reconstruction, and biophysical analysis of a respiratory motor circuit isolated in vitro. Journal of Neuroscience. 2008; 28:2353–2365. [PubMed: 18322082]
36. Ono T, Ishiwata Y, Inaba N, Kuroda T, Nakamura Y. Modulation of the inspiratory-related activity of hypoglossal premotor neurons during ingestion and rejection in the decerebrate cat. Journal of Neurophysiology. 1998; 80:48–58. [PubMed: 9658027]
37. Travers JB, DiNardo LA, H K. Medullary reticular formation activity during ingestion and rejection in the awake rat. Experimental Brain Research. 2000; 130:78–92. [PubMed: 10638444]
38. Chen Z, Travers SP, Travers JB. Muscimol infusions in the brain stem reticular formation reversibly block ingestion in the awake rat. American Journal of Physiology: Regulatory, Intergrative, and Comparative Physiology. 2001; 280:R1085–R1094.
39. Depuy SD, Kanbar R, Coates MB, Stornetta RL, Guyenet PG. Control of breathing by raphe obscurus serotonergic neurons in mice. Journal of Neuroscience. 2011; 31:1981–1990. [PubMed: 21307236]
40. Doi A, Ramirez JM. Neuromodulation and the orchestration of the respiratory rhythm. Respiratory Physiology & Neurobiology. 2008; 164:96–104. [PubMed: 18602029]
41. Hattox AM, Li Y, Keller A. Serotonin regulates rhythmic whisking. Neuron. 2003; 39:343–352. [PubMed: 12873389]
42. Van der Maelen CP, Aghajanian GK. Intracellular studies showing modulation of facial motoneurone excitability by serotonin. Nature. 1980; 287:346–347. [PubMed: 7421993]
43. Harish O, Golomb D. Control of the firing patterns of vibrissa motoneurons by modulatory and phasic synaptic inputs: A modeling study. Journal of Neurophysiology. 2010; 103:2684–2699. [PubMed: 20200122]
44. Saito Y, Ezure K, Tanaka I, Osawa M. Activity of neurons in ventrolateral respiratory groups during swallowing in decerebrate rats. Brain Development. 2003; 25:338–345. [PubMed: 12850513]
45. Kleinfeld D, Sachdev RNS, Merchant LM, Jarvis MR, Ebner FF. Adaptive filtering of vibrissa input in motor cortex of rat. Neuron. 2002; 34:1021–1034. [PubMed: 12086648]

Additional references for online methods

46. Lewis TL Jr, Mao T, Svoboda K. Myosin-dependent targeting of transmembrane proteins to neuronal dendrites. Nature Neuroscience. 2009; 12:568–576.
47. Uchida N, Mainen ZF. Speed and accuracy of olfactory discrimination in the rat. Nature Neuroscience. 2003; 6:1224–1229.
48. Ganguly K, Kleinfeld D. Goal-directed whisking behavior increases phase-locking between vibrissa movement and electrical activity in primary sensory cortex in rat. Proceedings of the National Academy of Sciences USA. 2004; 101:12348–12353.
49. O'Connor DH, Clack NG, Huber D, Komiyama T, Myers EW, Svoboda K. Vibrissa-based object localization in head-fixed mice. Journal of Neuroscience. 2010; 30:1947–1967. [PubMed: 20130203]
50. Shusterman R, Smear MC, Koulakov AA, Rinberg D. Precise olfactory responses tile the sniff cycle. Nature Neuroscience. 2011; 14:1039–1044.
51. Knutsen PM, Derdikman D, Ahissar E. Tracking whisker and head movements in unrestrained behaving rodents. Journal of Neurophysiology. 2005; 93:2294–2301. [PubMed: 15563552]
52. Hill DN, Curtis JC, Moore JD, Kleinfeld D. Primary motor cortex reports efferent control of vibrissa position on multiple time scales. Neuron. 2011; 72:344–356. [PubMed: 22017992]
53. Deschênes M, Timofeeva E, Lavallee P. The relay of high frequency sensory signals in the whisker-to-barreloid pathway. Journal of Neuroscience. 2003; 23:6778–6787. [PubMed: 12890771]

54. Paxinos G, Watson C, Pennisi M, Topple A. Bregma, lambda and the interaural midpoint in stereotaxic surgery with rats of different sex, strain and weight. Journal of Neuroscience Methods. 1985; 13:139–143. [PubMed: 3889509]

55. Ghosh S, Larson SD, Hefzi H, Marnoy Z, Cutforth T, Dokka K, Baldwin KK. Sensory maps in the olfactory cortex defined by long-range viral tracing of single neurons. Nature. 2011; 472:217–220. [PubMed: 21451523]

56. Paxinos, G.; Watson, C. The Rat Brain in Stereotaxic Coordinates. San Diego: Academic Press; 1986.

57. Ito T, Oliver DL. Origins of glutamatergic terminals in the inferior colliculus identified by retrograde transport and expression of VGLUT1 and VGLUT2 genes. Frontiers of Neuroanatomy. 2010; 4:135.

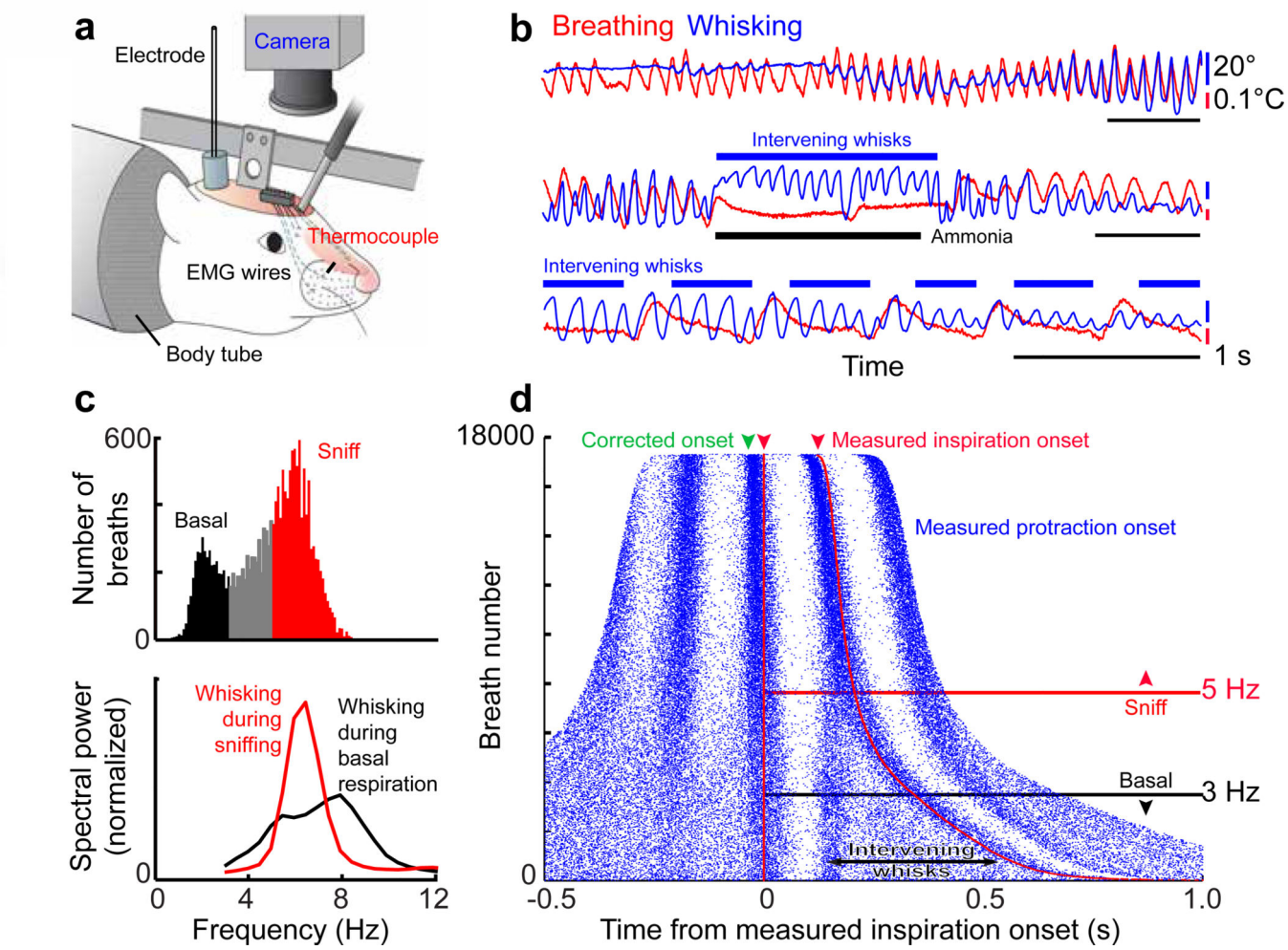

Figure 1. Coordination of whisking and breathing

(a) Procedures to measure whisking, breathing, and associated electrophysiology in headrestrained rats.

(b) Simultaneous measurement of vibrissa position (blue) and breathing (red). Protraction and inspiration are upward.

(c) Histogram of instantaneous breathing frequencies (top) delineates the classification of breaths below 3 Hz as basal respiration and those above 5 Hz as sniffs. The spectral power of whisking (bottom) is plotted during periods of basal respiration (black) as well as sniffing (red).

(d) Rasters of inspiration onset times (red) and protraction onset times (blue) relative to the onset of inspiration for individual breaths are ordered by the duration of the breath; green arrow represents the 30 ms lead of inspiratory drive to facial muscles as opposed to the measured inspiration. Whisks and inspiration onset times are significantly correlated during both sniffing and basal respiration ($p < 0.01$).

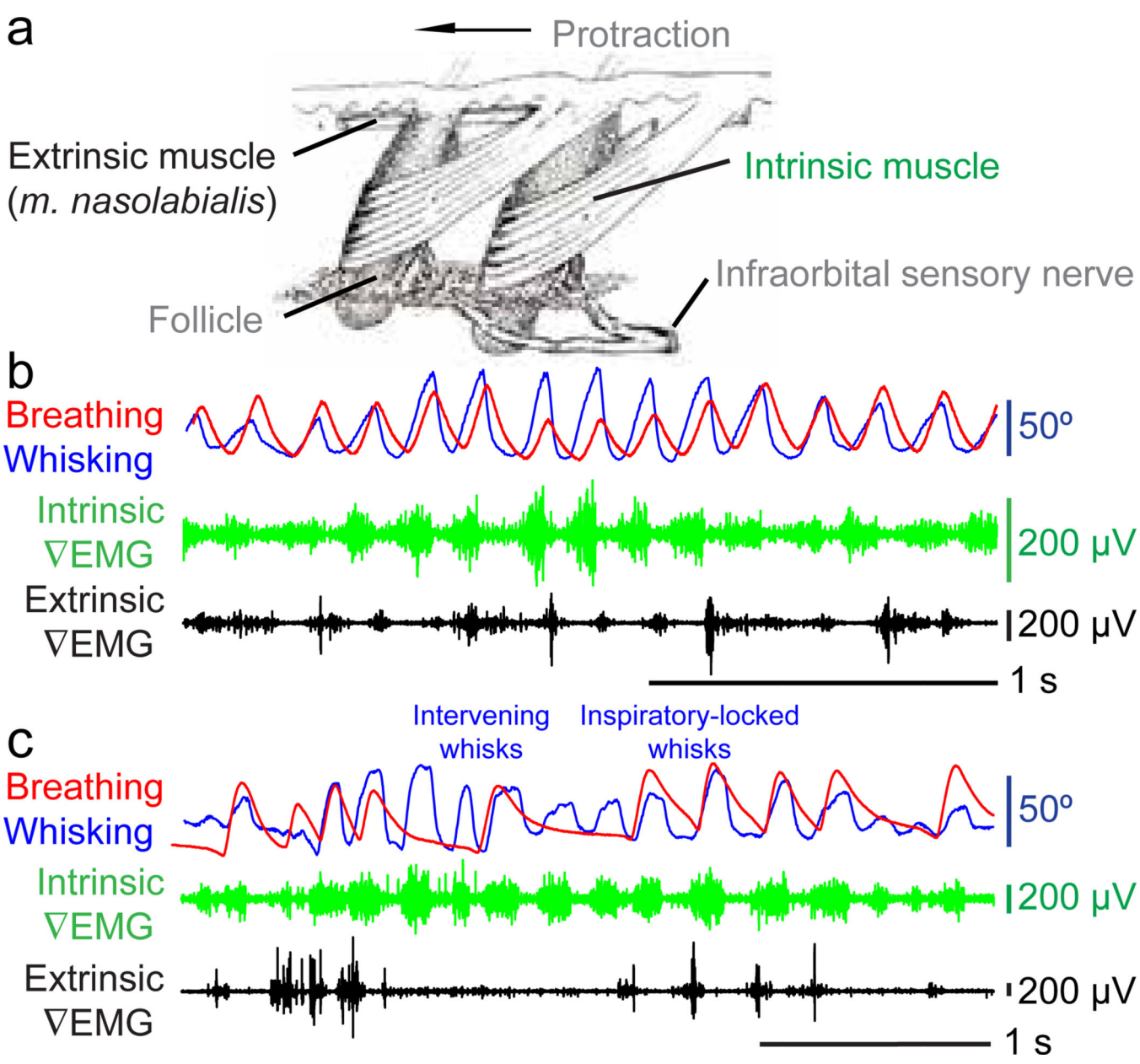

Figure 2. Facial muscle activity during whisking and breathing

(a) The musculature responsible for vibrissa and mystacial pad motion; adapted from Dorfl[24].

(b) Vibrissa motion (blue), breathing (red), and intrinsic (green) and extrinsic (black) ∇EMG activity during whisking and sniffing.

(c) The same activity during whisking and mixed basal respiration and sniffing.

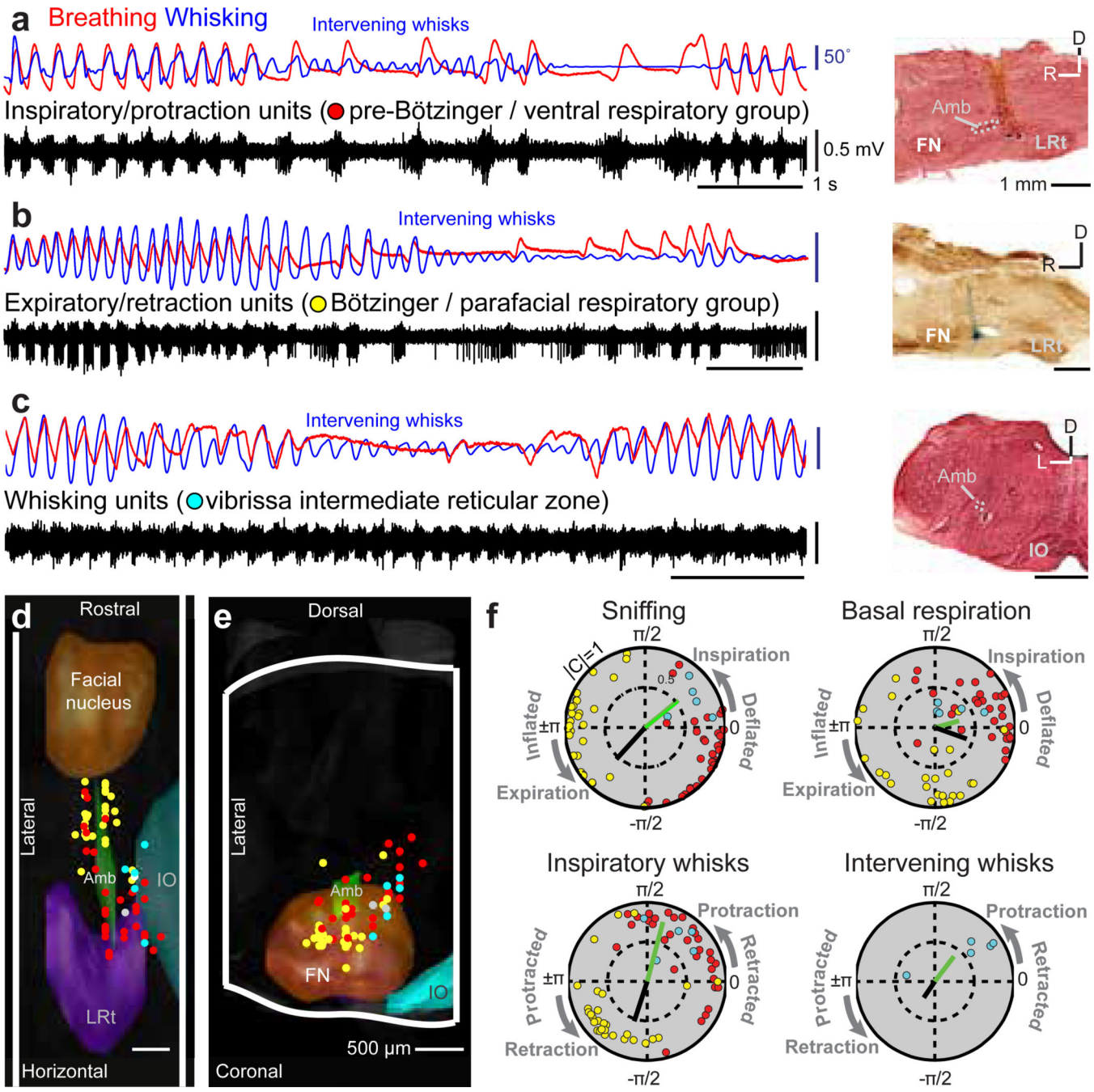

Figure 3. Activity in medullary respiratory centers during breathing and whisking

(a) Concurrent recordings of breathing (red), whisking (blue), and multiunit activity (black) in the preBötzinger complex. The location of the recording site is labeled with Chicago sky blue and is shown in a sagittal section counterstained with neutral red. LRt denotes the lateral reticular nucleus, FN the facial nucleus, Amb the *ambiguus* nucleus, and IO the inferior olive.

(b) Multiunit spike activity in the Bötzinger complex. The section is counterstained for cytochrome oxidase.

(c) Multiunit spike activity in the vibrissa zone of the intermediate reticular formation. The section is counterstained with neutral red.

(d,e) The recording sites for all data imposed on a three dimensional reconstruction of the medulla. Whisking units are located dorsomedially to the preBötzinger complex in the IRt. Two units whose spiking had no relation to breathing or whisking are shown in white.

(f) Polar plots of the magnitude (0 to 1 radial coordinate) and phase (angular coordinate) of the coherence between multiunit spiking activity and measured behaviors at the peak frequency for each behavior, *i.e*., 2 Hz for basal respiration, 6 Hz for sniffing and inspiratory whisks, and 8 Hz for intervening whisks (Fig. 1c). Only units with significant coherence ($p < 0.01$) are shown and correspond to the point in panels d to f. The coherence between the measured behavior and the ∇EMG of the intrinsic muscles (green bar) and *Nasolabialis* muscle ∇EMG (black bar) are shown.

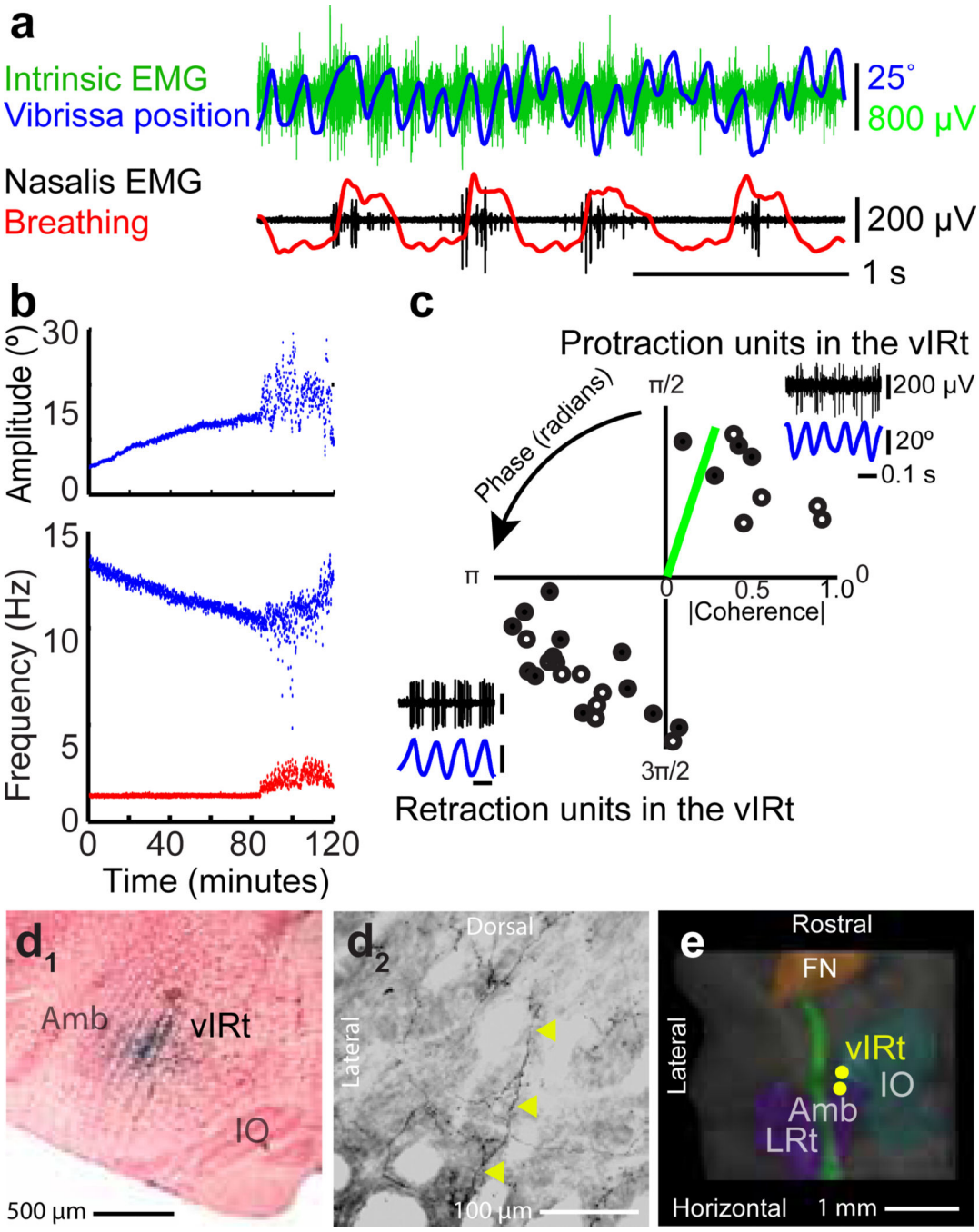

Figure 4. Injection of kainic acid in the medullary reticular formation induces whisking

(a) Vibrissa motion (blue), breathing (red), intrinsic (green) and extrinsic (black) ∇EMG.

(b) Time-course of kainic-acid induced whisking. Instantaneous peak-to-peak amplitude (top) and frequency (bottom) of vibrissa motion (blue) and frequency of breathing (red). The animal starts to wake by 100 minutes.

(c) Polar plots of the coherence between spiking activity and vibrissa motion at the peak frequency of whisking (8.8 Hz median); only units with statistically significant coherence (32 of 33 units, $p < 0.01$) are shown. Open circles represent multiunit activity and closed

circles represent single units. The green bar represents the coherence of the ∇EMG for the intrinsic muscle (panel b) with vibrissa motion. (Inserts) Spiking activity of neuronal units in the vIRt (black) in relation to vibrissa motion (blue).

(d_1) One of the locations that corresponded to a units in panel c, labeled via ionophoretic injection of Neurobiotin™ through the recording electrode.

(d_2) Axons (yellow arrows) and terminals in the ventral lateral division of the facial nucleus labeled after Neurobiotin™ injection at the recording site in panel d_1.

(e) Three dimensional reconstruction of the labeled recording locations for the units in panel d.

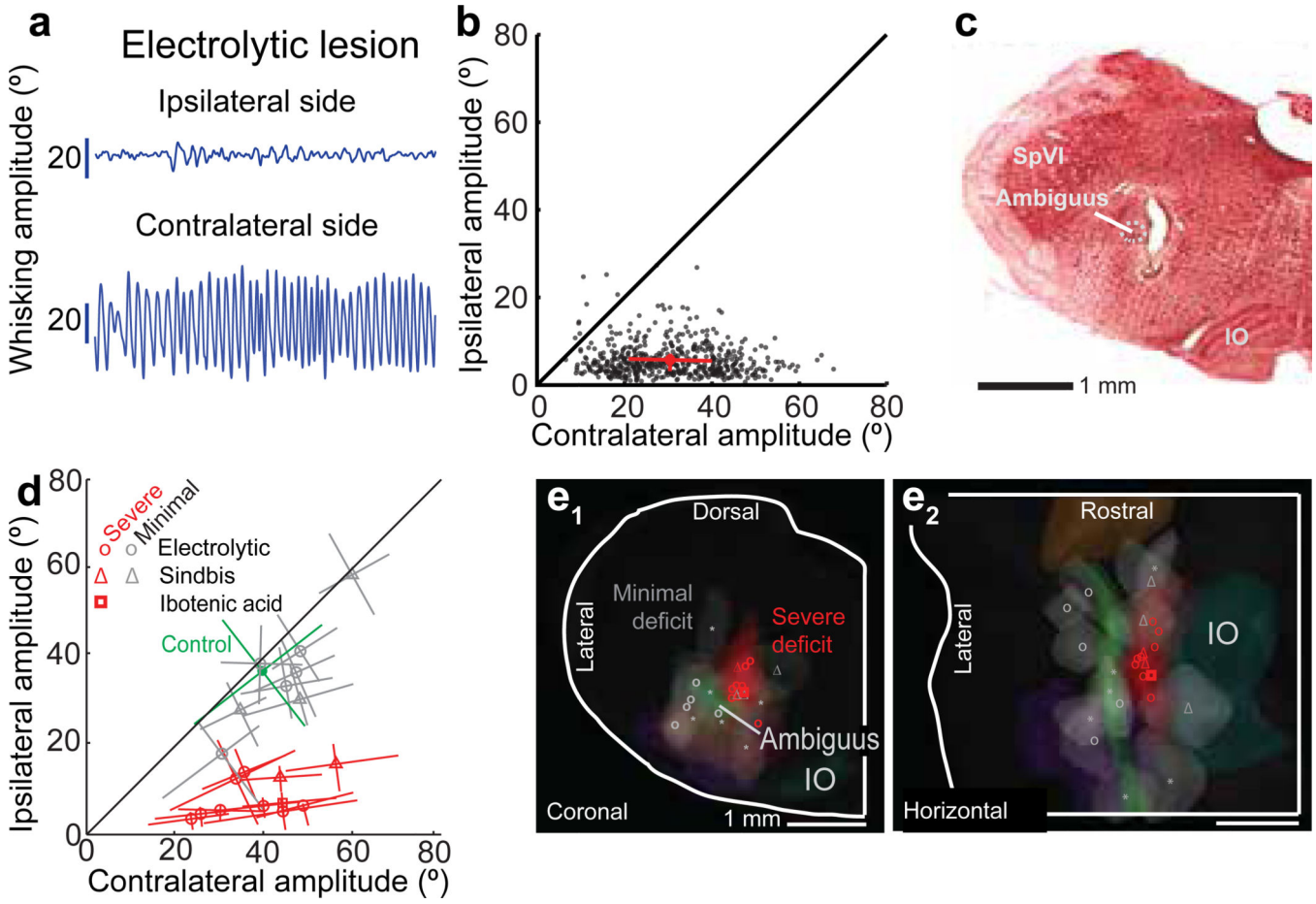

Figure 5. Lesion of the vIRt impairs ipsilateral whisking

(a) Example of whisking bout following an electrolytic lesion.

(b) Scatter plot of ipsilateral versus contralateral whisk amplitudes reveals the functional completeness of the lesion; each dot represents one whisk, circle represents the mean, and lines represent the inter-quartile range.

(c) Histological analysis confirms that the lesion is in the vIRt; coronal section stained with neutral red.

(d) Composite results for a subset of lesions (19 rats) where vibrissa position was tracked; lines are central quartiles. Symbols correspond to the method of lesion. Results were scored by the severity of the ipsilateral whisking deficit: severe (red), for > 50 % reduction as in panels a and b, or minimal (gray), < 50 % reduction. Whisking of a non-lesioned control rat is shown in green.

(e_1–e_2) Lesion sites were mapped onto a three dimensional reconstruction of the medulla and selected anatomical substructures, as in Figure 4f. The lesion centroids are denoted with the symbols in panel d and have a median volume of 0.2 μL. Sites marked with an asterisk (six rats) represent additional lesions not shown in panel d where animals were observed to have minimal whisking deficits by visual inspection.

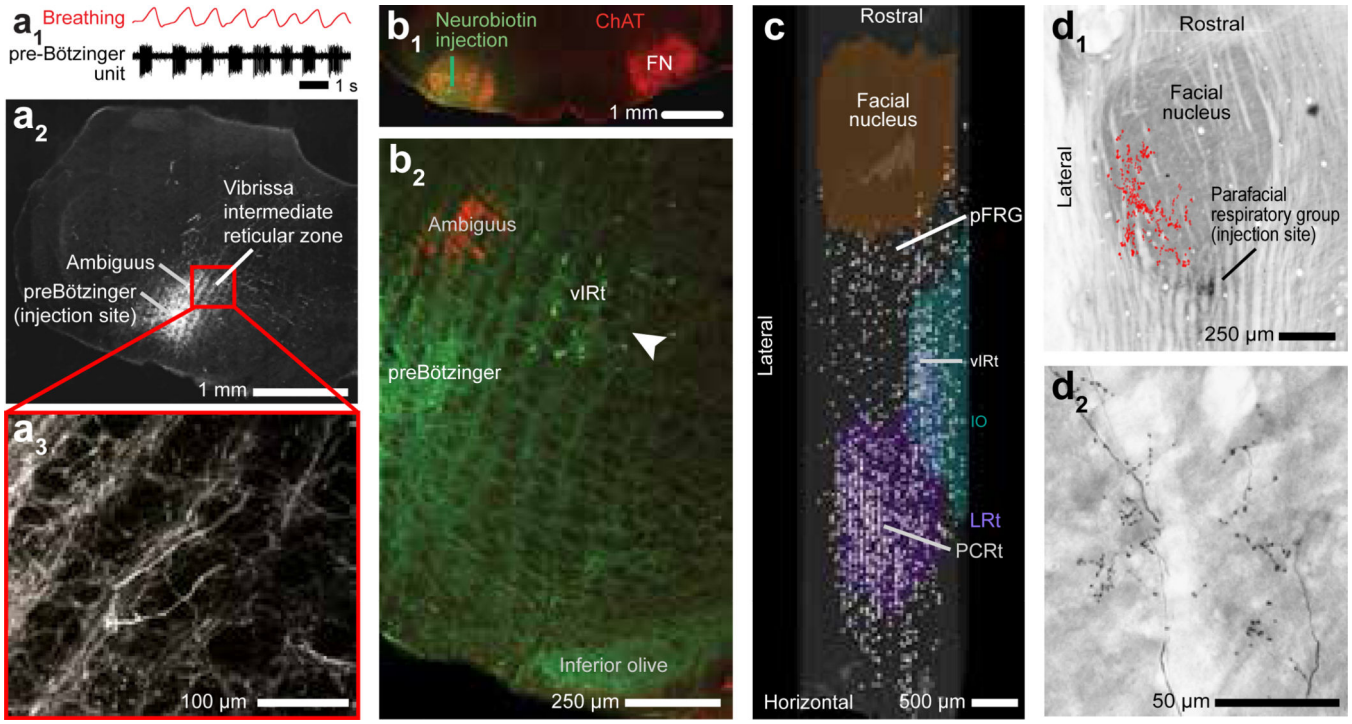

Figure 6. Anatomical evidence for connections between respiratory and whisking zones

(a_1–a_3) Recording of a single inspiratory unit in the preBötzinger complex, together with breathing (panel a1). Injection of biotinylated dextran amine through the same pipette (panel a2) leads to anterograde labeling of axons and terminals in the vIRt (panel a_3); panels a_2 and a3 are coronal sections.

(b_1,b_2) Injection of Neurobiotin™ (green) into the facial nucleus (FN) (panel b_1) retrogradely labels neurons in the vIRt (panel b_2; white arrow). Labeling with α-choline acetyl-transferase highlights motoneurons in the facial and *ambiguus* nuclei (red).

(c) Compendium of the locations of cells that were retrogradely labeled from the facial nucleus with Neurobiotin™, superimposed on a three dimensional reconstruction of the medulla. Note labeled cells in the vIRt, located between coronal planes −12.5 and −13.0 mm relative to bregma, that span ~ 200 µm along the lateral-medial axis. pFRG denotes the parafacial respiratory group and PCRt the parvocellular reticular nucleus.

(d_1,d_2) Injection of Neurobiotin™ into the parafacial region labels terminals in the dorsolateral aspect of the facial nucleus (panel e1). Individual axons and terminals are seen in panel e2, while a compendium across three consecutive sections is summarized in panel e1 (red dots). Horizontal sections stained for cytochrome oxidase.

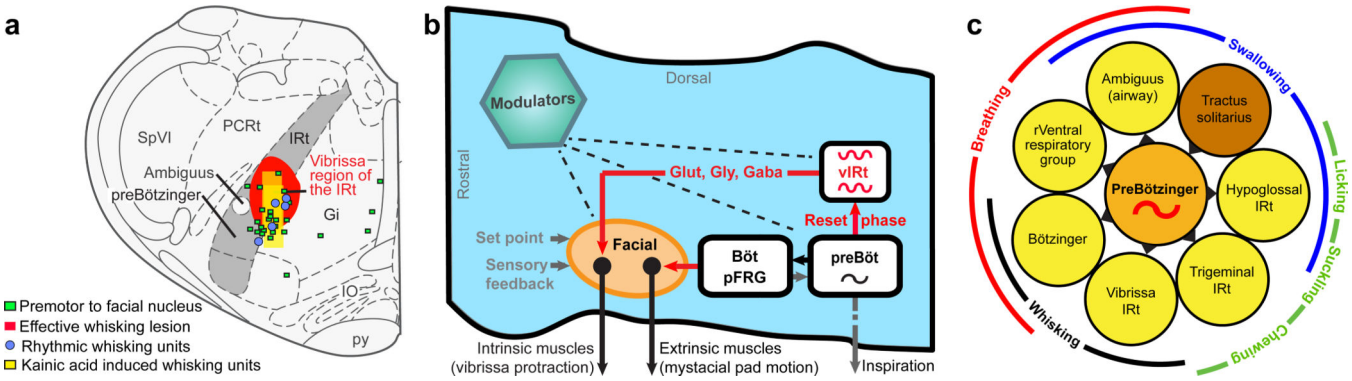

Figure 7. The whisking rhythm generator circuit in the broader context of orofacial behaviors

(a) Summary of evidence for a rhythm generator in the vibrissa zone of the intermediate band of the reticular formation (IRt; gray). This region contains units that fire in phase with all whisking events in freely behaving animals as well as when whisking is induced by microinjection of kainic acid. This region also contains cells that project to the facial nucleus, and lesions of this area severely disable whisking on the ipsilateral side.

(b) Model of the medullary circuitry that generates whisking in coordination with breathing.

(c) Summary of all premotor nuclei (yellow) that are known to receive rhythmic drive from the preBötzinger complex (orange), or conjectured to receive input based on anatomical projections, along with a potential resetting circuit (brown). The nuclei subserve shared oral facial behaviors, as demonstrated here for whisking (black) and breathing (red).